JOURNAL OF RAMAN SPECTROSCOPY
J. Raman Spectrosc. 2005; **36**: 648–656
Published online in Wiley InterScience (www.interscience.wiley.com). DOI: 10.1002/jrs.1356

JRS

Adaptive silver films for surface-enhanced Raman spectroscopy of biomolecules

Vladimir P. Drachev,[1] Mark D. Thoreson,[1]* Vishal Nashine,[3] Eldar N. Khaliullin,[1] Dor Ben-Amotz,[2] V. Jo Davisson[3] and Vladimir M. Shalaev[1]

[1] School of Electrical and Computer Engineering, Purdue University, West Lafayette, Indiana 47907, USA
[2] Department of Chemistry, Purdue University, West Lafayette, Indiana 47907, USA
[3] Department of Medicinal Chemistry and Molecular Pharmacology, Purdue University, West Lafayette, Indiana 47907, USA

Received 4 November 2004; Accepted 15 February 2005

The interaction of biological molecules with a typical substrate for surface-enhanced Raman scattering (SERS) often leads to their structural and functional changes. In this paper we describe SERS substrates, called adaptive silver films (ASFs), in which the biomaterial and the substrate act in concert to produce excellent Raman enhancement through local restructuring of the metal surface while at the same time preserving the properties (such as conformational state and binding activity) of the analyte. These adaptive substrates show great promise for SERS spectroscopy of many different types of biomolecules, and we provide several current examples of their use. Copyright © 2005 John Wiley & Sons, Ltd.

KEYWORDS: protein sensing; metal nanostructures; surface-enhanced Raman scattering; insulin; protein binding reaction

INTRODUCTION

The detection of biomolecules by optical means is of particular interest in areas such as pharmaceuticals, bio-warfare agent detection and many others. Raman scattering has been used as a detection method for molecule sensing in many cases previously, with one of the main advantages being that Raman spectra are, in essence, fingerprints of molecules. This is of particular interest for bio-applications, where specificity of detection is important. Surface-enhanced Raman scattering (SERS) provides even greater detection sensitivity than conventional Raman spectroscopy,[1–3] and it is quickly gaining traction in the study of biological molecules adsorbed on a metal surface.[4–12] SERS spectroscopy allows for the detection and analysis of minute quantities of analytes because it is possible to obtain high-quality SERS spectra at sub-monolayer molecular coverage as a result of the large scattering enhancements. SERS has also been shown to be sensitive to molecular orientation and to the distance from the metal surface.[13] Hence SERS is well suited for biomolecule studies in which specificity and sensitivity to the conformational state and orientation of the molecule are very important.

*Correspondence to: Mark D. Thoreson, School of Electrical and Computer Engineering, Purdue University, 465 Northwestern Avenue, West Lafayette, Indiana 47907, USA.
E-mail: mthoreso@purdue.edu
Contract/grant sponsor: Inproteo.

The SERS enhancement mechanism originates in part from the large local electromagnetic fields caused by resonant surface plasmons that can be optically excited at certain wavelengths for metal particles of different shapes or closely spaced groups of particles.[14–21] For aggregates of interacting particles, which are often structured as fractals, plasmon resonances can be excited in a very broad spectral range.[22] In addition to electromagnetic field enhancement, metal nanostructures and molecules can form charge-transfer complexes that provide further enhancement for SERS.[23–29] The resulting overall enhancement depends critically on the particle or aggregate nanostructure morphology[22,30–36] and it can be as high as 10^5–10^8 for the area-averaged macroscopic signal and 10^{10}–10^{15} within the local resonant nanostructures.

A variety of structures have been found to be appropriate for SERS, including roughened metal electrodes,[1–3] aggregated films,[15] metal islands of different morphology[14,15,17–20] and semicontinuous films near the percolation threshold.[37–39] Among SERS-active substrates, vacuum-evaporated nanostructured metal films are well suited for SERS mechanism studies and have a high potential for applications.[14–20,24,39–43] The effect on the metal film due to deposition rate, mass thickness and thermal annealing have been studied in detail previously.[18,40–43] We found recently that silver films fabricated at a certain range of evaporation parameters allow fine rearrangement of their local structure under protein deposition.[44,45] Such substrates, which we will refer to as

adaptive to distinguish them from static-structure substrates, provide large SERS enhancement and appear to preserve the functionality of biomolecules. As we have predominantly used silver as the metal in our films in order to take advantage of theoretically higher enhancements from silver, we refer to these special substrates as adaptive silver films (ASFs).

In this paper, we discuss some specific properties of adaptive substrates and provide several examples of their uses for protein sensing. We also describe a further development of this type of substrate to improve SERS signals by the addition of a sublayer of bulk metal.

EXPERIMENTAL

ASF fabrication

The ASFs are typically fabricated on a dielectric substrate under vacuum evaporation with an electron beam. This process involves the controlled deposition of semicontinuous films on the initial dielectric substrate. Microscope glass slides (from Fisher) were cut into 25×25 mm sections for use as initial substrates. The cut slides were cleaned through several steps, including multiple solvent rinses, a piranha (H_2O_2–$3H_2SO_4$) acid bath, rinsing in 18 MΩ deionized water and drying with pressurized gaseous nitrogen. Silver shot from Alfa Aesar (99.9999%, 1–3 mm) and SiO_2 pellets from Lesker (99.995%, cut quartz) were used for fabrication of the ASFs on the glass substrates. Thin-film deposition was performed in a modified Varian electron beam evaporator with an initial pressure inside the system of $\sim 10^{-7}$ Torr (1 Torr = 133.3 Pa). The film thickness and deposition rate were monitored with a quartz crystal oscillator. The glass sections were covered first with a 10 nm sublayer of silica followed by a silver layer (10–13 nm) deposited at a rate of 0.05 nm s^{-1}. Fabricated substrates were stored in a desiccated environment and were typically used within 1 month of fabrication. Because of the very thin layer thickness, the silver is not continuous across the dielectric substrate. Specifically, during the silver deposition process small isolated metal granules are formed first on the dielectric substrate. As the silver coverage increases through further deposition, the granules coalesce on the substrate surface. The deposition process is stopped before a continuous silver layer is formed, resulting in various sizes of silver particles and their aggregates. For multi-layer substrates, a preliminary layer of bulk silver (80 nm) was deposited below the silica sublayer.

Biomolecule analytes and depositions

Recombinant human insulin and insulin lispro were provided by Eli Lilly. Our samples were prepared from Zn-insulin crystals; the crystals were dissolved, aliquoted into the vials and the vials were lyophilized. Typically, 2–4 μl of 1 μM insulin solution containing 0.1 mM HCl was deposited on a substrate and then allowed to dry in a 45° inclined position (see the subsections below for further details). The dried biomolecule spots are typically 2 mm^2 in size and are stable under typical laboratory handling conditions. Subsequent washing in either deionized water or Tris-buffered saline (TBS) solution removed the silver from those areas not affected by the protein drops. However, the protein spots showed no changes under washing, indicating that the protein solution has mediated a stabilization of the silver film during the drying process.

For antibody–antigen binding studies, several different molecule solutions were used. Anti-FLAG M2 monoclonal antibody (fAb) and bacterial alkaline phosphatase/C-terminal FLAG-peptide fusion (fBAP) were purchased from Sigma-Aldrich. For binding activity validation experiments, Cy3 dye-conjugated monoclonal anti-FLAG antibody (Cy3-fAb), and horseradish peroxidase (HRP)-conjugated anti-mouse IgG were obtained from Sigma-Aldrich. Bacterial alkaline phosphatase (BAP) without the FLAG peptide was generated by enterokinase-catalyzed cleavage of FLAG peptide (see the subsections below). Aliquots (2 μl) of 0.5 μM solutions of fBAP and/or BAP were manually deposited on the ASF substrate and incubated for 2 h under shaking conditions at room temperature. The substrates were then rinsed with TBS and probed with fAb in TBS. The excess fAb was rinsed with TBS followed by washing with water.

In order to study the effect of a bulk silver sublayer on the SERS signal for three analytes, we obtained SERS spectra for three biomolecules on both standard two-layer ASF substrates and three-layer ASF substrates, fabricated as mentioned above. The analytes used were human insulin (Eli Lilly), anti-human interleukin 10 antibody (anti-IL10, from Pierce), and anti-IL10 incubated with rhodamine 6G dye (R6G, from Sigma-Aldrich). For insulin we used the same solution parameters as mentioned above. For the anti-IL10 experiment, 2 μl droplets were deposited manually on both substrate types. After allowing the spots to dry, the substrates were washed in TBS solution containing 0.1% Tween-20 for 20 min. In the anti-IL10/R6G experiment, 2 μl of 1 μM anti-IL10 were deposited manually on the substrates and allowed to dry. The substrates were then incubated in 60 ml of 10 nM R6G in TBS solution for 35 min. SERS spectra were obtained for both substrate types, and the intensities were compared for the three analytes.

Insulin solution preparation

Insulin was dissolved in 1 mM HCl prepared by dilution with deionized water of ultra-pure grade. Insulin concentrations were determined from absorbance measurements at 280 nm.[44,45] The solution was then diluted with dilute HCl or water. Typically, 2–4 μl of 1 μM insulin solution containing 0.1 mM HCl was deposited on a substrate and then allowed to dry in a 45° inclined substrate position. The protein distribution in the deposited spot was obtained with an Alpha-step 200 profilometer (Tencor Instruments). The spot typically consists of an outer ring and a central part.[44,45] The average protein density in the spot is $\sim$200 fmol mm^{-2} calculated

from a 3 μl volume, 1 μM concentration, and 14 mm^2 area. A surface density density estimate of about 80 ± 20 fmol mm^{-2} was obtained for the central area of the spot.

BAP preparation

f-BAP protein was diluted to 500 ng ml^{-1} in dilution buffer (10 mM Tris–HCl, 10 mM $CaCl_2$, pH 8.0) and 20 U of enterokinase were added followed by incubation at 37 °C for 24 h. The completion of the reaction was followed by slot-blot (Schleicher und Schüll) on a nitrocellulose membrane. The free peptide was removed using Ultrafree0.5 (5 kDa MWCO) spin concentrators (Millipore). Water used in these preparations was obtained from Burdick and Jackson. The protocol followed in the antibody–antigen experiments were similar to the Western blotting procedure provided by Sigma. Tris-buffered saline (TBS) consisted of 50 mM Tris, HCl (pH 8.0), 0.138 M NaCl and 2.7 mM KCl.

SERS spectra collection

SERS spectra were collected at a laser wavelength of 568 nm, 1 mW power and an exposure time of 200 s and were subjected to background subtraction using a Fourier method. For insulin, the SERS specific intensity of the Phe peak at 1003 cm^{-1} was about 33 counts s^{-1} mW^{-1}.[44,45] The specific intensities for fAb and fBAP SERS signals were ~4–7 counts s^{-1} mW^{-1} measured at the 1000 cm^{-1} peak. For fAb and fBAP studies, SERS spectra were collected and compared after each washing step to observe any differences caused by a binding (or loss) event. In all cases, a four-wavelength Raman system was used which consists of an Ar–Kr ion laser (Melles Griot), a laser band-path holographic filter (to reject plasma lines), two Super-Notch Plus filters to reject Rayleigh scattering (Kaiser Optical Systems), focusing and collection lenses, an Acton Research 300i monochromator with a grating of 1200 grooves mm^{-1} and a nitrogen-cooled charge-coupled device (CCD) detector (1340 × 400 pixels) (Roper Scientific). An objective lens (*f*/1.6) provided a collection area with a diameter of ~180 μm. Collected light was delivered to a monochromator via a fiber bundle. The spectral resolution was ~3 cm^{-1} with a laser power of ~1 mW and an exposure time of 100–200 s.

RESULTS AND DISCUSSION

The characterization and use of the ASF substrates are discussed in this section. Characterization involved analysis of the ASFs by many methods, including UV–visible spectrometry, field emission scanning electron microscopy (FE SEM), adhesion testing, atomic force microscopy (AFM) and SERS enhancement. We will begin by discussing the results of several of these methods individually, and we will also include a brief discussion on the visible characteristics of ASF substrates before and after analyte solution deposition. Following the characterization results, we demonstrate the usefulness of the ASF substrates for SERS detection of biomolecules by providing two example experimental results.

Adaptive silver films

Although most SERS substrates have a predefined and static metal-dielectric nanostructure, this is not in general the best case for obtaining an optimal Raman signal from any particular analyte. Experiments reveal that a variation of evaporated metal films produces substrates with new adsorption and restructuring features that are important for SERS detection and analysis of biomolecules.[44,45] In particular, the restructuring involves competition between two processes. A protein solution (e.g. in TBS) can slightly dissolve the Ag particle surfaces to make them movable. At the same time, stabilization by proteins can occur, in which the protein molecules coat the silver particles and thereby protect the particles on the surface from dissolving in the buffer.

Along with the advantages provided by being SERS-active, these adaptive films address three additional issues. First, direct adsorption of biomolecules on a metal surface often leads to their significant structural (denaturation) and/or functional changes.[5,8,46,47] Hence not all substrates are biocompatible while it is of great interest to study biomolecules in their native forms with functionality preserved. Second, any particular metal nanostructure with a fixed morphology cannot perfectly match different analytes and provide the optimal SERS in all cases owing to the differences in analyte sizes. Finally, biomolecular research often involves several washing procedures to remove non-binding or excess agents. This washing can also remove metal nanoparticles with medium to low adhesion to the substrate. Adaptive silver films allow protein-mediated restructuring of the nanoparticles, which makes it possible to address all three issues simultaneously. Specifically, biomolecules adsorb on the metal surface without significant structural changes (*soft* adsorption), the silver film stabilizes on the surface, which makes the biomolecule–metal combinations resistant to washing, and the SERS signal improves for a given set of particles.

Film stabilization

A representative view of an ASF substrate before and after biomolecule deposition is shown in Fig. 1. After deposition and drying, subsequent washing of the substrate in either deionized water or TBS solution removed the silver from those areas not affected by the biomolecule solution drops. However, the protein spots show no changes after washing, as clearly seen in Fig. 1, indicating that the protein solution has mediated stabilization of the silver film during the drying process. From this we conclude that the biomolecules stabilize the silver film, allowing the silver film to remain in place even through washing procedures. This stabilization does not occur for spots without biomolecules (proteins), indicating that the biomolecules themselves play a key

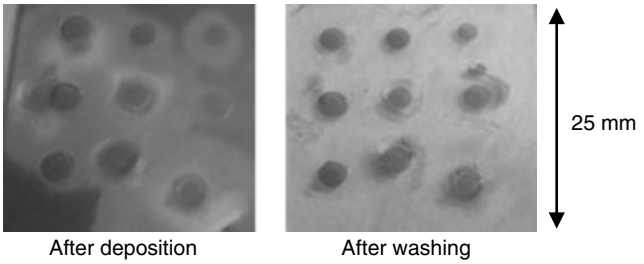

Figure 1. ASF film with protein spots before (top) and after (bottom) washing. The spots are roughly 2 mm^2 in size.

role in forming a stable complex with the silver particles. By varying the biomolecule and buffer concentrations, we observe that both factors are important in the formation of uniform, stabilized analyte spots. A lower biomolecule concentration (by roughly a factor of 10–20) in our deposition solution results in an almost transparent spot and hence no metal particles. In this case the solvent (buffer) may dissolve the metal particles, leaving merely silver salt on the substrate. Preliminary results from x-ray diffraction studies support this conclusion, and also indicate that the silver particles coated with biomolecules are not oxidized (as would be expected for silver exposed to air). The silver dissolving process occurring when the biomolecules have not coated a silver particle may affect the interface between the silver particles and the silica sublayer, and hence it may decrease adhesion or even remove particles in solution. Deposition of the biomolecule solution without buffer reveals no visible changes to the film surface. We also verified in a preliminary experiment that film restructuring and stabilization can be accomplished with a synthetic polymer such as polyvinylpyrrolidone (PVP) in TBS solution.

UV–visible spectral analysis

Excitation of the collective electron oscillations (plasmons) in a metal nanostructure results in strong light and particle interaction, and such excitation eventually leads to increased absorption relative to a thick metal film. Near-ultraviolet and visible spectra were measured using a Lambda-35 spectrophotometer (Perkin-Elmer) to characterize the nanostructured films. In particular, the reflectance and absorbance spectra are compared to provide information on the film structure. The light impinging on a semicontinuous metal film will undergo transmission, reflection or absorption, with a small percentage (typically <5%) experiencing scattering. By measuring the intensity of light in each of these processes at different frequencies, one can judge whether the film structure supports resonant plasmon modes. At the frequencies where resonances occur, absorption increases. Typical UV–visible absorbance and reflectance spectra of an ASF substrate are similar in shape and have a maximum at around 500 nm with a broad wing into the longer wavelengths (see Plate 1). Reflection of these films is typically comparable to or slightly larger than absorption (by a factor of ~1–1.4 when both spectra are expressed in percent). Both the visible color of the film and the extinction spectrum change after analyte deposition, as shown in Plate 1. The spectrum inside the analyte spot typically shows a blue-shifted maximum, reduced slope of the long-wavelength wing and reduced extinction integrated over the 300–1100 nm spectral range.

FE SEM image analysis

One of the best ways to characterize the ASF substrates is in actually looking at the nanostructure of the metal film. A scanning electron microscope is potentially useful here, but such systems often exhibit charging issues for non-conductive samples such as our ASFs. Therefore, we employed an FE SEM system to image our samples on the nanoscale. Using such a device, it is possible to obtain excellent images of the ASF nanostructure and to determine changes in the nanostructure as a result of the analyte deposition and restructuring.

High-resolution FE SEM images were obtained through MAS (Raleigh, NC, USA). Representative nanostructure images before and after analyte deposition are shown in Fig. 2 for an 11 nm ASF. For the samples used in Fig. 2, fAb antibody molecules in a concentration of 1 μM in TBS solution were deposited on the ASF substrate. The images show metal nanoparticles and their aggregates in white and dielectric material in dark gray or black. The large-sized

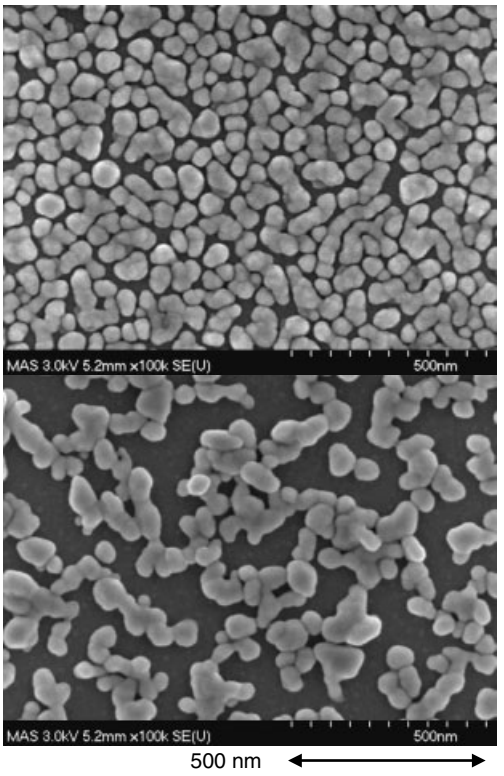

Figure 2. FE SEM images of an ASF (11 nm mass thickness) inside spot before (top) and after protein deposition and washing (bottom).

particles have complicated shapes and an internal structure. Figure 2 clearly shows that the film experiences nanoscale restructuring inside the biomolecule spot, where groups of closely spaced metal nanoparticles are formed. This is in contrast to the film outside the biomolecule spot, where rather disintegrated particles are typical. A metal filling factor can also be calculated from FE SEM images. Defined as the ratio of the area covered by metal to the total area, the filling factor is lower inside the biomolecule spot than outside (see Fig. 2). Decreases in the integrated extinction and in the metal filling factor both suggest a decrease in the silver mass thickness caused by biomolecule deposition. This indicates that some of the metal nanoparticles have been dissolved in solution. It is interesting that extinction changes primarily after protein deposition and does not change much after subsequent washing.

Atomic force microscopy

Whereas FE SEM data give us information on the lateral structure of the semicontinuous film, AFM analysis yields insight into the vertical structure of the ASF. AFM images were acquired with a Dimension 3100 instrument (DI Veeco) using a 10 nm Si tip. A typical AFM height profile for an ASF is shown in Fig. 3. AFM analysis indicates that the particle height is typically less than the lateral plane size. The maximum height exceeds the mass thickness which is expected for nanostructured film. An example of an 8 nm film shows a maximum height of ~30 nm with r.m.s. deviations from the mean in the range 5–7 nm. At the same time, the ASF is uniform on the micrometer scale and higher such that this film is very homogeneous within a laser spot of ~80–100 μm.

Adhesion testing

The adhesion of the metal film to the glass substrate is important to the function of our ASF films. If adhesion is too high, no discernible restructuring will occur. At the same time, very low adhesion yields poor film quality and stability before analyte deposition. A quantitative adhesion analysis of these semicontinuous films is difficult to implement, but qualitative estimates of adhesion were performed with the common tape test.[48] In this test, the tape was attached to the film and then pulled off. Absorption and reflection measurements before and after the tape test indicate the relative level of adhesion of the film to the glass substrate. A comparison of silver substrates with and without an SiO_2 sublayer show that adhesion of silver on glass is poor, whereas the Ag–SiO_2–glass substrate shows good adhesion in the tape test. The changes in absorption/reflection spectra were <5% for the Ag–SiO_2–glass substrate.[44,45] In the case of high adhesion (such as including an adhesion-promoting titanium sublayer), the deposition of the biomolecule solution does not lead to spot color changes or structural modifications, and typically little or no SERS is observed.

X-ray photoelectron spectroscopy (XPS)

XPS is used to analyze the elemental species on a sample surface based on the photoelectron effect. This analysis technique is capable of probing ~10 nm of a sample surface. In the case of ASF samples, this depth corresponds approximately to the metal film thickness, and we can estimate that the analysis results include predominantly data from the outer metal layer along with any biomolecules deposited on the film surface. By measuring kinetic energy of the photoelectrons at a given photon energy (1486.6 eV, in this case), one can detect the binding energy spectrum. The binding energies of the peaks are characteristic for each element. The peak areas can be used to determine the relative composition of the sample surface. The shape of each peak and the binding energy can be slightly altered by the chemical state of the emitting atom. Hence XPS can also provide chemical bonding information. In our case, the high energy resolution spectra provide information on the oxidation state of silver and the relative composition of different carbon bonds, including hydrocarbons, C—C, C—O (C—N) bonds and O—C═O.

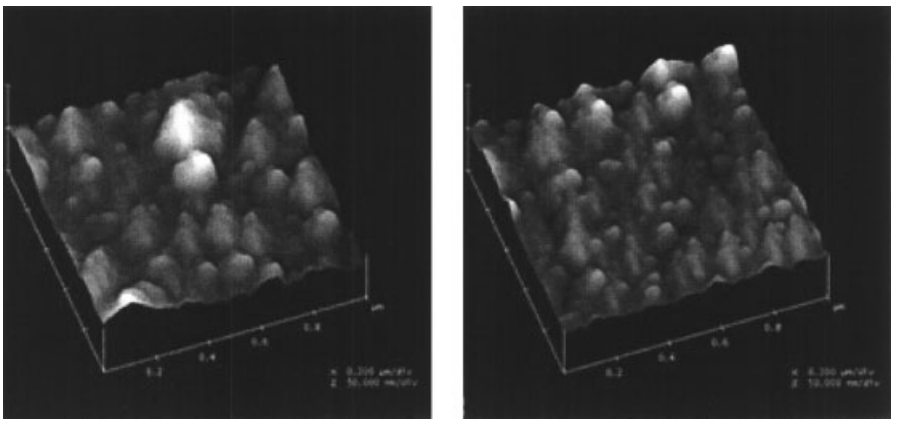

Figure 3. AFM images of an 8 nm ASF before (left) and after deposition (right).

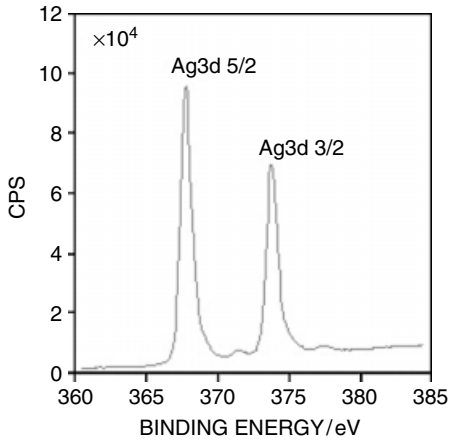

Figure 4. XPS high energy resolution spectrum of Ag 3d region.

XPS analysis was performed through Rocky Mountain Laboratories for several ASF samples. The results indicate the relative amounts of elemental species in our metal films and in the analytes deposited on those films. In our vacuum-evaporated films studied with XPS, ~25–30% of the composition is silver and carbon makes up 30–35%. Oxygen (25–28%), silicon (12–14%) and sodium (<2%) are also present on the surface. The silicon, oxygen in part and sodium are most likely attributable to the glass or silicon dioxide sublayers in the ASF substrate structure. Representative XPS high energy resolution spectrum of the Ag 3d region is shown in Fig. 4. An important result is that the silver on the substrate is still in its metal state (Ag $3d_{5/2}$ peak position is at 368.5 eV) without oxidation after about 8 weeks from fabrication (the Ag $3d_{5/2}$ peak is shifted to 367.0–367.4 eV). The presence of metal-state silver indicates that the substrates are reasonably stable over time, which is very helpful for production and storage of the substrates. Deposition of a protein solution makes the silver surface partially oxidize.

XPS analysis also indicates that there is carbon contamination on the substrates. This is typical of vacuum-evaporated films, and very difficult to avoid. We also note that there is no contamination in our samples from other evaporation sources used previously in the vacuum evaporator (such as gold or titanium), which indicates that the evaporator system is relatively clean and the source purity is very high.

SERS enhancement

The biomolecule-mediated restructuring illustrated by FE SEM images in Fig. 2 results in aggregates of closely spaced particles covered with biomolecules. This is in contrast to the rather disintegrated particles of the initial film before analyte deposition. Depending on the mass thickness of the initial film, small or large fractal-like aggregates can be formed. The analyte SERS signal, normalized to unit metal mass coverage, is comparable for both the small and large aggregates that we examined. SERS enhancement is high enough to detect a monolayer of analyte.[44,45] Note that an aggregated structure provides conditions for both electromagnetic and chemical SERS enhancements. Even small aggregates provide strong electromagnetic enhancement in the visible and near infrared regions, as has been shown for polarization non-linearities[49] and SERS.[31] Large aggregates typically have a fractal morphology, which is known to provide a particularly strong SERS signal.[22,39] In addition, the first molecular layer may also produce conditions to make an optical tunnel current possible, either through the molecule at the point of nearest approach between two particles[39] or through a system operating as a molecular tunnel junction between particles across a vibrating molecular bridge.[50] Hence the adaptive feature of our films creates cavity sites enclosed by two or more particles, producing places that are optimal for Raman enhancement. It is even more important that the cavity sites are naturally filled with proteins as a result of restructuring.

The measured macroscopic enhancement factor for insulin on our ASF substrate relative to normal Raman of insulin on quartz is about 3×10^6,[44,45] which is among the largest observed in the literature for random metal-dielectric films [10^5 for nitrobenzonate[42] and 5.3×10^5 for *trans*-1,2-bis(4-pyridyl)ethylene[19]].

It is important to note that, in general, non-adaptive films (without restructuring) are created by optimizing either evaporation parameters (sublayer, deposition rate, increased mass thickness) or biomolecule solution contents. This means that non-adaptive substrates should be tailored to specific biomolecule solutions, or vice versa. Clearly, such changes can affect metal structures or biomolecule adsorption, which makes it impossible to compare SERS results on adaptive films directly with those from non-adaptive films. Regardless, from analysis of FE SEM images and SERS enhancement results, the observation is that there is no detectable SERS without restructuring.

Biomolecule detection with ASFs

In order to demonstrate the use of ASF substrates for SERS of biomolecules, we provide two examples. We first discuss ASF experiments involving the detection of insulin analogs, then we cover the detection of antibody–antigen binding events using ASF substrates.

Insulin isomers

Insulin is a protein consisting of 51 amino acids split into two chains, as shown in Fig. 5, and is a glucose regulation agent in the bloodstream. In general, protein sensing using Raman spectroscopy provides important structural information on conformational changes. Changes between native and denatured insulin in the solid form and spectral features of proinsulin and insulin fibrils were studied previously.[51–53] Signatures of allosteric conformation changes in hexameric insulin have been assessed using

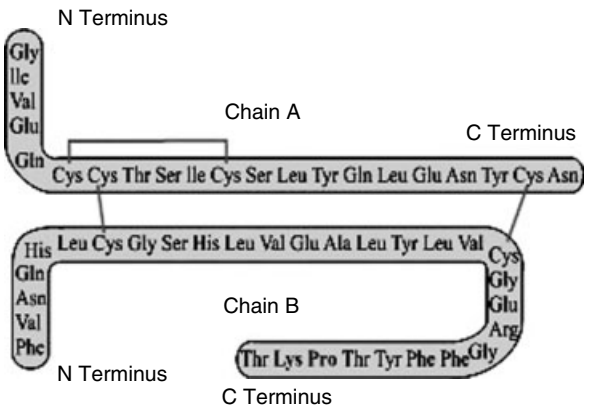

Figure 5. Primary structure of human insulin, with two chains of 51 amino acids.

Raman difference spectroscopy.[54] In our insulin analog experiments, we demonstrated that ASFs can be used for the observation of differences in SERS spectra of recombinant human insulin and insulin lispro at very low protein surface densities (see Refs 44 and 45 for details). As mentioned previously, the ASFs modify their local nanostructure under protein deposition so that the conformational state of insulins is preserved and SERS is improved.

The experiments examined differences in the Raman spectra of two insulin isomers, human insulin and its analog insulin lispro. These two insulins differ only in the interchange of two neighboring amino acids; specifically, the propyl–lysyl sequence at the C-terminus of the B-chain in insulin lispro is inverted as compared with human insulin (see Fig. 5, near the C-terminus). This propyl–lysyl switch leads to conformational changes at the C- and N-termini and has an important clinical effect for diabetes treatment. In this experiment we used Raman difference spectroscopy, which is a general method of probing protein structure for comparison between closely related proteins,[55] which we extended to SERS in order to study the spectral features of insulin conformation. In our experiments, all insulin vibration modes are enhanced by approximately the same factor. This makes the SERS spectra similar to the conventional Raman spectra in liquid and solid forms and simplifies the analysis.[44,45]

The difference in SERS spectra for the two insulins (see Plate 2) was detected at a sub-monolayer density of 80 fmol mm^{-2}, with only 25 amol in the probed area. Our SERS spectra indicate that insulin is adsorbed on the metal surface through the N-termini. This suggests a possible scenario for insulin and silver particle interaction on the surface and helps us understand the restructuring mechanism in this case. Because of specific Cl^- adsorption, silver particles acquire excess negative charges and attract the positively charged N-termini of the insulin molecules. Insulin hexamers have six N-termini of their B-chains exposed to the hexamer surface, three at the top and three at the bottom.[44,45] Hence insulin hexamers can serve as coupling agents and induce the surface restructuring within a protein spot. Since human insulin and its analog have the same set of side-chains and differ only in conformational states, the observed SERS difference indicates the preservation of the conformational state with the use of our ASF substrates.

Antibody–antigen binding

We have also studied ASF substrates for use in antibody–antigen (Ab–Ag) binding detection. Our results show that SERS substrates based on ASFs allow direct, label-free SERS detection of Ab–Ag binding at a monolayer level. Antigen–antibody binding events result in distinct SERS spectral changes, as shown in Plate 3. It is important to note that the ASF substrates also allow independent *in situ* binding activity validation using traditional chemiluminescence and fluorescence methods. We performed such validation and confirmed that antigens and antibodies retain their binding properties on our SERS-active ASF substrate. As with insulin, we find that the deposited biomolecules (antibodies or antigens, in this case) restructure and stabilize the ASF so that the protein binding activities are preserved and, in parallel, SERS is improved.

Label-free detection using ASF substrates produces unique advantages relative to prior optical binding detection methods (typically based on different types of labels) such as scintillation counting,[56] electrochemical,[57] enzymatic,[58] fluorescence[59,60] and chemiluminescence methods.[61] An additional feature of the ASFs is an ability to employ various detection methods on the same substrate, such as label-free SERS, chemiluminescence, fluorescence and further analysis of proteins retrieved from the substrate spot.

Multi-layer ASF structures

A metal nanostructured film positioned near a mirror-like metal surface with a sandwiched dielectric layer can show dramatic change in the film's optical properties.[62–64] The localized plasmon resonances supported by the constituents of metal island films experience a frequency shift when placed in close proximity to a conducting surface.[62] The strong dependence of the spectral position of the reflectivity minimum on the spacer thickness is caused by enhanced absorption.[63] The enhancements in absorption and elastic scattering[64] are likely associated with the existence of strongly enhanced local fields. These changes are attributed to an enhancement of the dipole–dipole interaction between the different particles mediated by propagating modes that are supported by a layered sample,[64] interaction between dipole and its own image[62] and interference effects between waves reflected from different interfaces in the sample.[63]

We employed such a sandwich structure to increase further the SERS signal from ASF-based biosensors. The sandwich structure [Plate 4(b)] contains a bulk silver layer (80 nm) deposited on glass, then a layer of SiO_2 (10 nm) and finally a 12 nm nanostructured silver film. Relative

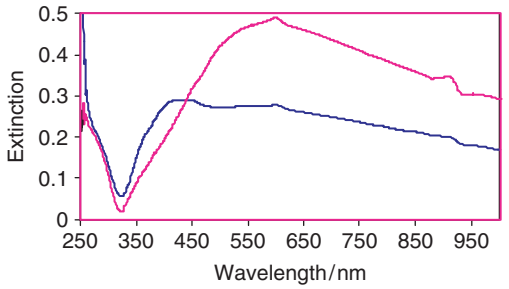

Plate 1. Typical extinction spectra outside (red) and inside the protein spot (blue).

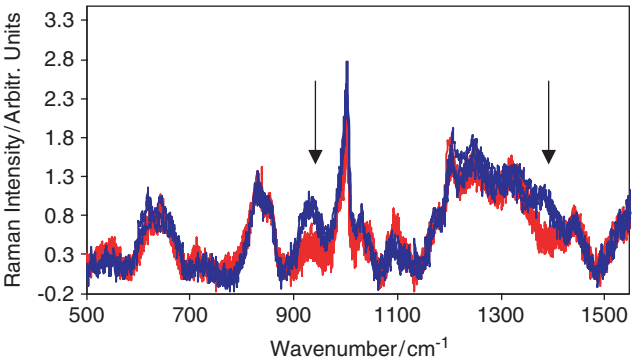

Plate 2. Human insulin (blue) and insulin lispro (red) SERS spectra (collected over three spots each). Arrows indicate main spectra difference areas.

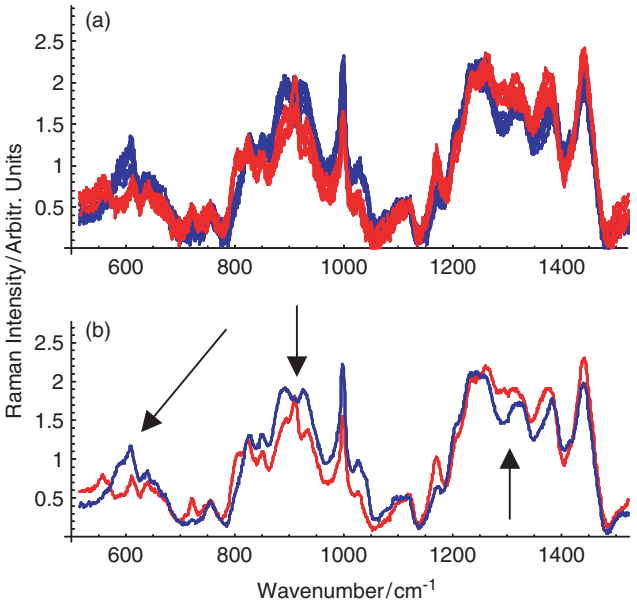

Plate 3. SERS spectra of antigen (blue) and antigen after incubation in an antibody solution (red): (a) nine spectra, each obtained from three spots; (b) averages, with arrows indicating main spectra change areas.

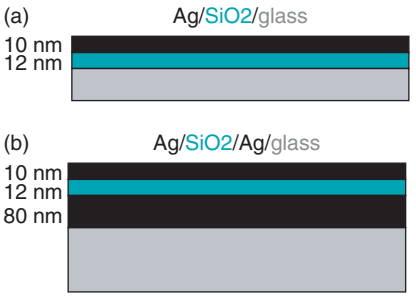

Plate 4. Vertical layer structure for ASF substrates: (a) two-layer structure; (b) multi-layer structure.

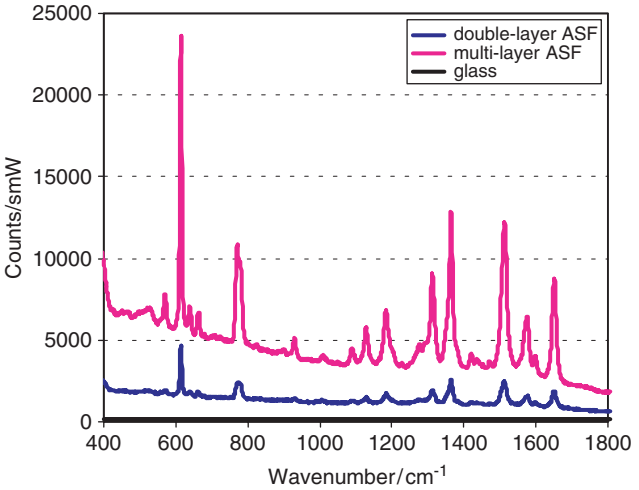

Plate 5. R6G SERS spectra from double-layer and multi-layer ASF substrates.

Table 1. SERS signals for two types of ASF substrates (intensities in counts per second per milliwatt)

	Two-layer $Ag-SiO_2-glass$	Multi-layer $Ag-SiO_2-Ag-glass$
Insulin	Max. 7	28–38
Antibody (anti-human interleukin 10)	20–25	80–100
Antibody incubated with R6G	3500	16000

to the usual ASF structure [Plate 4(a)], it has only an additional sublayer of bulk metal. The bulk silver layer provides an additional enhancement of the local fields caused by the interaction between the fields around the metal nanostructures and their images in the bulk layer, and by far-field interactions between the metal particles. We performed test experiments with these multi-layer structures using three analytes: human insulin, anti-human interleukin 10 and anti-human interleukin 10 incubated with 1 nM R6G. Plate 5 illustrates the relative increment of the SERS intensity for R6G inside an antibody (anti-human interleukin 10) spot. Table 1 shows specific intensities (in counts per second per milliwatt) of a characteristic peak of Ab and R6G from the sandwich ASF sample and the usual ASF structure. Note that in our experiments with insulin we observed 28–38 counts s^{-1} mW^{-1} from the sandwich structure (vs 1.5–4 counts s^{-1} mW^{-1} for the particular substrate used for comparison and 7 counts s^{-1} mW^{-1} for maximum signal over all samples). From the data in Table 1, we conclude that the multi-layer sandwich structure provides a signal increment of at least 4–5.

CONCLUSION

In summary, the nanostructured ASFs demonstrate advantages over static-structure SERS substrates. The characterization of these films leads to the conclusion that ASFs experience fine restructuring under biomolecule deposition such that conformation and functionality are preserved. In addition, the biomolecule-mediated restructuring produces excellent conditions for SERS enhancement. The interaction of the silver film with the biomolecule solution acts to stabilize the system, making it resistant to wash processes.

Examples show that ASFs preserve the secondary structure of insulin and have a high SERS sensitivity in detecting conformational distinctions of nearly identical insulin isomers. In addition, we find that SERS substrates based on ASFs can be used for direct, label-free detection of protein binding at a monolayer level. Finally, ASF substrates allow independent validation for Ab-Ag binding by conventional chemiluminescence and fluorescence methods and show great promise for detection and analysis of biomolecules, even at very low surface densities.

Experiments with a multi-layer structure consisting of a bulk metal layer below the ASF structure reveal a promising way to improve further the sensitivity of SERS-based ASF biosensors.

Acknowledgment

This research was sponsored in a part by a grant from Inproteo, NSF grant HRD-0317722 and NASA grant NCC-31035.

REFERENCES

1. Fleischmann M, Hendra PJ, McQuillan AJ. *Chem. Phys. Lett.* 1974; **26**: 163.
2. Jeanmaire DJ, Van Duyne RP. *J. Electroanal. Chem.* 1977; **84**: 1.
3. Albrecht MG, Creighton JA. *J. Am. Chem. Soc.* 1977; **99**: 5215.
4. Vo-Dinh T. *Trends Anal. Chem.* 1998; **17**: 557.
5. Bauer G, Stich N, Schalkhammer TGM. In *Methods and Tools in Biosciences and Medicine: Analytical Biotechnology*, Schalkhammer TGM (ed). Birkhauser Verlag: Basel, 2002; 253.
6. Sibbald MS, Chumanov G, Cotton TM. *J. Electroanal. Chem.* 1997; **438**: 179.
7. Vo-Dinh T, Stokes DL, Griffin GD, Volkan M, Kim UJ, Simon MI. *J. Raman Spectrose.* 1999; **30**: 785.
8. Brown KR, Fox AP, Natan MJ. *J. Am. Chem. Soc.* 1996; **118**: 1154.
9. Shafer-Peltier KE, Haynes CL, Glucksberg MR, Van Duyne RP. *J. Am. Chem. Soc.* 2003; **125**: 588.
10. Cao YWC, Jin R, Mirkin CA. *Science* 2002; **297**: 1536.
11. Cao YC, Jin R, Nam JM, Thaxton CS, Mirkin CA. *J. Am. Chem. Soc.* 2003; **125**: 14 676.
12. Grubisha DS, Lipert RJ, Park HY, Driskell J, Porter MD. *Anal. Chem.* 2003; **75**: 5936.
13. Moskovits M. *Rev. Mod. Phys.* 1985; **57**: 783.
14. Moskovits M. *J. Chem. Phys.* 1978; **69**: 4159.
15. Chen CY, Burstein E, Lundquist S. *Solid State Commun.* 1979; **32**: 63.
16. McCall SL, Platzman PM, Wolff PA. *Phys. Lett. A* 1980; **77**: 381.
17. Chen CY, Burstein E. *Phys. Rev. Lett.* 1980; **45**: 1287.
18. Bergman JG, Chemla DS, Liao PF, Glass AM, Pinczuk A, Hart RM, Olson DH. *Opt. Lett.* 1981; **6**: 33.
19. Weitz DA, Garoff S, Gramila TJ. *Opt. Lett.* 1982; **7**: 168.
20. Ritchie G, Chen CY. In *Surface Enhanced Raman Scattering*, Chang PK, Furtak TE (eds). Plenum Press: New York, 1982; 361.
21. Yang WH, Schatz GC, Van Duyne RP. *J. Chem. Phys.* 1995; **103**: 869.
22. Stockman MI, Shalaev VM, Moskovits M, Botet R, George TF. *Phys. Rev. B* 1992; **46**: 2821.
23. Otto A. *Surf. Sci.* 1978; **75**: 1392.
24. Pockrand I, Otto A. *Solid State Commun.* 1980; **35**: 861.
25. Persson BNJ. *Chem. Phys. Lett.* 1981; **82**: 56.
26. Adrian FJ. *J. Chem. Phys.* 1982; **77**: 5302.
27. Pandey PK, Schatz GC. *J. Chem. Phys.* 1984; **80**: 2959.
28. Lombardi JR, Birke RL, Lu T, Xu J. *J. Chem. Phys.* 1986; **84**: 4174.
29. Campion A, Kambhampti P. *Chem. Soc. Rev.* 1998; **27**: 241.
30. Nie S, Emory SR. *Science* 1997; **275**: 1102; *J. Phys. Chem. B* 1998; **102**: 493.
31. Kneipp K, Wang Y, Kneipp H, Perelman LT, Itzkan I, Dasari RR, Feld M. *Phys. Rev. Lett.* 1997; **78**: 1667.
32. Schatz GC, Van Duyne RP. In *Handbook of Vibrational Spectroscopy*, Chalmers JM, Griffiths RP (eds). Wiley: New York, 2002; 759.

33. Musick MD, Keating CD, Keefe MH, Natan MJ. *Chem. Mater.* 1997; **9**: 1499.
34. Michaels AM, Nirmal M, Brus LE. *J. Am. Chem. Soc.* 1999; **121**: 9932.
35. Haynes CL, Van Duyne RP. *J. Phys. Chem.* 2003; **107**: 7426.
36. Prodan E, Radloff C, Halas NJ, Nordlander P. *Science* 2003; **302**: 419.
37. Gadenne P, Gagnot D, Masson M. *Physica A* 1997; **241**: 161.
38. Sarychev AK, Shalaev VM. *Phys. Rep.* 2000; **335**: 275.
39. Shalaev VM. *Nonlinear Optics of Random Media: Fractal Composites and Metal-Dielectric Films*. Springer: Heidelberg, 2000.
40. Davies JP, Pachuta SJ, Cooks RG, Weaver M. *Anal. Chem.* 1986; **58**: 1290.
41. Schlegel VL, Cotton TM. *Anal. Chem.* 1991; **63**: 241.
42. Van Duyne RP, Hulteen JC, Treichel DA. *J. Chem. Phys.* 1993; **99**: 2101.
43. Vogel E, Kiefer W, Deckert V, Zeisel D. *J. Raman Spectrosc.* 1998; **29**: 693.
44. Drachev VP, Khaliullin E, Thoreson MD, Davisson VJ, Shalaev VM. *J. Phys. Chem. B* 2004; **108**: 18 046.
45. Drachev VP, Thoreson MD, Khaliullin EN, Sarychev AK, Zhang D, Ben-Amotz D, Shalaev VM. *Proc. SPIE* 2003; **5221**: 76.
46. Holt RE, Cotton TM. *J. Am. Chem. Soc.* 1989; **111**: 2815.
47. Yang M, Chang FL, Thompson M. *Anal. Chem.* 1993; **65**: 3713.
48. Eckertova L. *Physics of Thin Films*. Plenum Press: New York, 1977.
49. Drachev VP, Perminov SV, Rautian SG, Safonov VP. In *Optical Properties of Nanostructured Random Media*, Shalaev VM (Ed). Springer: Berlin, 2001; 113.
50. Michaels AM, Jiang JJ, Brus LE. *J. Phys. Chem. B* 2000; **104**: 11 965.
51. Yu NT, Liu CS. *J. Am. Chem. Soc.* 1972; **94**: 3250.
52. Yu NT, Liu CS, O'Shea DC. *J. Mol. Biol.* 1972; **70**: 117.
53. Yu NT, Jo BH, Chang RCC, Huber JD. *Arch. Biochem. Biophys.* 1974; **160**: 614.
54. Ferrari D, Diers JR, Bocian DF, Kaarsholm NC, Dunn MF. *Biopolym. Biospectrosc.* 2001; **62**: 249.
55. Callender R, Deng H, Gilmanshin R. *J. Raman Spectrosc.* 1998; **29**: 15.
56. Gutcho S, Mansbach L. *Clin. Chem.* 1977; **23**: 1609.
57. Hayes FJ, Halsall HB, Heineman WR. *Anal. Chem.* 1994; **66**: 1860.
58. Butler JE. *J. Immunoassay* 2000; **21**: 165.
59. Vuori J, Rasi S, Takala T, Vaananen K. *Clin. Chem.* 1991; **37**: 2087.
60. Xu YY, Pettersson K, Blomberg K, Hemmila I, Mikola H, Lovgren T. *Clin. Chem.* 1992; **38**: 2038.
61. Brown CR, Higgins KW, Frazer K, Schoelz LK, Dyminski JW, Marinkovich VA, Miller SP, Burd JF. *Clin. Chem.* 1985; **31**: 1500.
62. Holland WR, Hall DG. *Phys. Rev. Lett.* 1984; **52**: 1041.
63. Leitner A, Zhao Z, Brunner H, Aussenegg FR, Wokaun A. *Appl. Opt.* 1993; **32**: 102.
64. Stuart HR, Hall DG. *Phys. Rev. Lett.* 1998; **80**: 5663.